JOURNAL OF SOLID STATE CHEMISTRY 103, 228–239 (1993)

Synthesis and Characterization of Ba_2VO_4 with the β-Ca_2SiO_4 Structure: Comparison with Sr_2VO_4

GUO LIU AND J. E. GREEDAN

Institute for Materials Research, McMaster University, Hamilton, Ontario, Canada L8S 4M1

Received June 4, 1992; in revised form September 8, 1992; accepted September 14, 1992

Phase-pure Ba_2VO_4 has been synthesized by hydrogen reduction of a mixture of $Ba_3V_2O_8$ and 20% excess $BaCO_3$ at 1200–1250°C, and its crystal structure, designated as β-Ba_2VO_4, refined using a combination of powder neutron and X-ray diffraction data. It is monoclinic, space group $P2_1/n$ (no. 14), with a = 6.0191(7) Å, b = 7.6494(7), c = 10.465(1), β = 92.39(1)°, and V = 481.4(2) Å^3 from Guinier X-ray diffraction data. β-Ba_2VO_4 is isostructural with β-Ca_2SiO_4. The structure is closely related to β-K_2SO_4 and consists of isolated VO_4^{4-} tetrahedra and loosely bonded $Ba(1)O_{10}$ and $Ba(2)O_9$ polyhedra. Its magnetic behavior can be approximated as an $S = \frac{1}{2}$ infinite Heisenberg linear chain. The crystal structure and magnetic properties of the β-Ba_2VO_4 are compared with those of the structurally related high-temperature form of Sr_2VO_4 (β-Sr_2VO_4). Reexamination of the crystal structure of the latter discloses that one of the V(IV) atoms has a rare trigonal bipyramidal coordination and that this atom is weakly bonded to a VO_4^{4-} tetrahedron forming a $V_2O_8^{8-}$ dimer. The formation mechanism of β-Ba_2VO_4 and the possible existence of an orthorhombic form isostructural with β-K_2SO_4 are also discussed.

Introduction

We recently reported the synthesis and characterization of the metastable high-temperature form of Sr_2VO_4 (*1*) which contains VO_4^{4-} tetrahedra and is an interesting magnetic dimer. The high-temperature form of Sr_2VO_4, hereafter designated as β-Sr_2VO_4, is actually isostructural with Sr_2CrO_4 which has a superstructure of the β-K_2SO_4 type. The existence of VO_4^{4-} tetrahedra in β-Sr_2VO_4 recalls the well-known fact that tetrahedral coordination is the rule for the group IVA elements such as Ge and Si. In fact, the ternary alkaline earth silicates, M_2SiO_4 (M = Ca, Sr, Ba), have various types of crystal structures most of which are closely related to that of β-K_2SO_4 (*2–6*) and the known forms of Sr_2GeO_4 and Ba_2GeO_4 have the β-K_2SO_4 type structure (*3*). Tetrahedral TiO_4^{4-} is also known with two forms of Ba_2TiO_4 similar to those of Sr_2SiO_4 and Ca_2SiO_4 (*7, 8*). Ba_2VO_4 was reported to be isostructural with β-K_2SO_4 (*9, 10*), but no detailed structural data were available and its physical properties were unknown. Ba_2VO_4 would be structurally closely related to β-Sr_2VO_4 if it is indeed isostructural with β-K_2SO_4. In order to understand the effect of the size of the alkaline earth on the crystal chemistry and the magnetic behavior of VO_4^{4-}-containing oxides, we carried out a detailed study of the BaO–VO_2 system. In this paper the synthesis, crystal structure, and magnetic data of the new β-Ca_2SiO_4 type Ba_2VO_4 are presented.

0022-4596/93 $5.00

Experimental

Synthesis of Ba_2VO_4

$Ba_3V_2O_8$ was first made by firing an intimately ground and pelleted mixture of 3 : 1 $BaCO_3$ (Aesar, 99.9%) and V_2O_5 (Cerac, 99.9%) at 950°C in air for 24 hr. A 1 : 1 mixture of $Ba_3V_2O_8$ and $BaCO_3$ was ground with acetone, dried, and pelleted. The pellets were confined in a 1.25 cm diameter open molybdenum tube which was secured in an alumina boat. The mixture was heated in a flowing hydrogen gas atmosphere in a tubular furnace to 1200–1250°C within 4 hr, and then soaked for 24 hr. After cooling down, the pellets were pulverized, and 20% more molar $BaCO_3$ was added and intimately ground, pelleted, and finally fired in hydrogen at 1250°C again for 24 hr following the same procedure as the first firing. The final product was cooled slowly in the furnace.

X-ray and Neutron Diffraction

All specimens were examined routinely using a Guinier–Hägg camera (IRDAB XDC700) with Cu$K\alpha$1 radiation and a Si standard. The Guinier data were read with a computer-controlled automated LS-20 type line scanner (KEJ INSTRUMENTS, Täby, Sweden). Step-scanned X-ray powder diffraction data of Ba_2VO_4 suitable for profile refinement were collected in the range $15° < 2\Theta < 80°$ using a Nicolet I2 diffractometer with Cu$K\alpha$ radiation. Neutron diffraction data for powder Ba_2VO_4 were collected at the McMaster Nuclear Reactor using 1.3913 Å neutrons obtained by reflection from a Cu [200] monochromator. The X-ray data refinement was effected on a VAX computer using LHPM1 of Hill and Howard (*11*) which is a modified version of DBW3.2 due to Wiles and Young (*12*). Details of the neutron data collection and refinement methods have been described previously (*13*). Neutron scattering lengths (fm) used were 5.25, −0.382, and 5.805 for Ba, V, and O, respectively (*14*).

Magnetic Susceptibility Measurement and Thermogravimetrical Analysis

Susceptibility data were obtained using a Quantum Design SQUID magnetometer in the temperature range 4.5 to 300 K using pelleted specimens at an applied magnetic field of 0.2 T. Diamagnetic corrections were applied. Thermogravimetrical analysis (TGA) was performed with a Netzsch STA 409 Thermal Analyzer in flowing O_2 atmosphere at a heating rate of 5°C/min to 900°C.

Results and Discussion

The black grey Ba_2VO_4 prepared using 20% excess $BaCO_3$ was a single phase. Its thermal behavior is interesting. The specimen started oxidation above 200°C, with a maximum weight gain of 3.19(5)% at ~680°C, and then underwent a gradual weight loss upon further heating in O_2. Rapid weight loss occurred above 830°C and eventually it reached a plateau with extended heating at 900°C. These data suggest the formation of an intermediate, which was identified by powder X-ray diffraction as BaO_2 besides the expected product $Ba_3V_2O_8$. The observed final net weight gain, 1.80(5)%, is reasonably close to the calculated value of 2.05% for BaO and $Ba_3V_2O_8$ as the final products, and suggests that the Ba/V ratio is very close to 2/1 as expected for chemically pure Ba_2VO_4. The small discrepancy possibly indicates the existence of a trace amount of unreacted BaO or another form of it that was not seen by X-ray and neutron diffraction.

Crystal Structure

Powder X-ray diffraction peaks matched principally those reported for Ba_2VO_4 with apparent deviations in the low angle region, but more low angle reflection lines were observed in our experiment than reported previously (*9*, *10*). A least-squares refinement on the suggested orthorhombic lattice parame-

ters using 50 observed interplanar d-spacings gave a very poor fit, 33 values being rejected even though the refined unit cell parameters, a = 10.39(1) Å, b = 7.66(1) Å, and c = 6.063(5) Å, were close to those reported previously (*9*). Furthermore, the powder neutron profile of Ba_2VO_4 could not be refined based on the proposed orthorhombic β-K_2SO_4 model. The difference profile clearly revealed the mismatch of some peak positions, which is a common problem encountered when improper cell parameters are used. These results suggested that the true symmetry of Ba_2VO_4 was not orthorhombic, at least for the specimens prepared by the method described above.

An attempt was then made to index the observed d-spacings. The first 17 peaks can be indexed completely by TREOR (*15*) based on a monoclinic cell with lattice parameters a = 10.468(4) Å, b = 7.646(2) Å, c = 6.019(2) Å, and β = 92.39(3)° and high figures of merit, $M(17)$ = 29 and $F(17)$ = 41. No orthorhombic solution was obtained. A least-squares refinement based on this monoclinic cell with 42 observed d-spacings gave the final lattice parameters a = 10.465(1) Å, b = 7.6494(7) Å, c = 6.0191(7) Å, and β = 92.39(1)°, with rejection of only eight peaks due to ambiguous indexation caused by peak overlaps. Observed and calculated d-spacings and observed intensities are listed in Table I. The systematic extinction conditions suggested the space group $P2_1/n$. When appropriate permutations about the lattice parameters were made, the similarity between Ba_2VO_4 and the monoclinic forms of Ba_2TiO_4 (*7*), β-Ca_2SiO_4 (*5*), and β-Sr_2SiO_4 (*4*), all of which are isostructural and closely related to β-K_2SO_4, can be noticed immediately. The correctness of the structural model was confirmed by the subsequent profile refinements using both powder neutron and X-ray diffraction data. For convenience this new phase is designated as β-Ba_2VO_4 by analogy with the β phases of Ca_2SiO_4 and Sr_2SiO_4.

TABLE I

OBSERVED (GUINIER DATA) AND CALCULATED INTERPLANAR d-SPACINGS AND OBSERVED GUINIER INTENSITIES FOR β-Ba_2VO4

h	k	l	d_{cal}	d_{obs}	I_{obs}
1	0	−1	5.3097	5.3016	4.5
1	1	−1	4.3618	4.3588	6.8
0	1	2	4.3162	4.3161	3.1
0	2	1	3.5919	3.5885	10.9
1	1	−2	3.5652	3.5630	29.1
1	1	2	3.4507	3.4504	37.7
1	2	0	3.2273	3.2263	38.0
0	1	3	3.1716	3.1712	22.4
1	2	−1	3.1034	3.1024	63.6
0	2	2	3.0868	3.0864	54.5
1	0	−3	3.0716	3.0687	100.0
1	2	1	3.0645		
2	0	0	3.0069	3.0062	79.9
1	0	3	2.9624	2.9620	46.2
1	2	−2	2.7741	2.7734	6.5
1	2	2	2.7191	2.7193	10.0
0	2	3	2.5761	2.5765	25.8
2	1	−2	2.5081	2.5092	7.0
0	3	1	2.4772	2.4767	50.4
0	1	4	2.4735		
2	1	2	2.4283	2.4287	9.6
2	2	0	2.3639	2.3609	11.1
2	2	−1	2.3221	2.3200	10.4
1	1	−4	2.3200		
1	3	−1	2.2985	2.2980	3.2
2	2	1	2.2896	2.2900	12.6
1	3	1	2.2826	2.2824	4.6
1	1	4	2.2565	2.2558	4.4
2	1	−3	2.2247	2.2251	11.3
2	2	−2	2.1809	2.1807	30.8
0	2	4	2.1581	2.1584	5.4
2	1	3	2.1419	2.1421	14.0
2	2	2	2.1279	2.1286	16.6
0	3	3	2.0579	2.0578	7.4
0	1	5	2.0172	2.0176	16.1
2	2	−3	1.9868	1.9865	10.5
2	1	−4	1.9484	1.9481	2.8
0	4	0	1.9124	1.9129	5.8
2	3	1	1.9027	1.9029	8.6
2	3	−2	1.8390	1.8398	3.6
0	2	5	1.8348	1.8351	4.2
1	4	0	1.8224	1.8223	8.0
0	4	2	1.7960	1.7955	29.2
1	4	1	1.7915	1.7917	8.2
3	2	0	1.7755	1.7754	6.5
3	0	−3	1.7699	1.7706	12.4
3	2	−1	1.7612	1.7610	34.2
1	3	−4	1.7609		

TABLE I—*Continued*

h	k	l	d_{cal}	d_{obs}	I_{obs}
3	2	1	1.7399	1.7396	11.0
1	3	4	1.7326	1.7328	14.2
2	1	−5	1.7072	1.7072	14.6
3	0	3	1.7072		
3	2	−2	1.7004	1.7021	2.8
2	3	3	1.6791	1.6790	6.4
0	4	3	1.6766	1.6766	7.1
1	1	−6	1.6528	1.6528	7.6
3	1	−4	1.5884	1.5887	6.8
0	2	6	1.5858		
2	4	−2	1.5517	1.5521	5.0
3	3	1	1.5508	1.5496	3.0
1	3	5	1.5490		
4	0	0	1.5035	1.5036	11.5
2	4	−3	1.4770	1.4770	4.6
1	5	−1	1.4701	1.4704	3.2
0	5	2	1.4683	1.4684	4.6
1	5	1	1.4659	1.4660	7.1
2	4	3	1.4520	1.4522	4.2
2	3	−5	1.4436	1.4427	11.2
1	1	−7	1.4379	1.4384	3.8
3	4	0	1.3837	1.3837	3.2
2	2	6	1.3812	1.3812	3.6
4	2	1	1.3799	1.3693	5.2
3	3	−4	1.3696		
3	4	1	1.3666	1.3669	6.9
3	3	4	1.3305	1.3304	5.1
1	5	−4	1.2954	1.2950	2.8
4	0	4	1.2804	1.2802	3.2
0	6	0	1.2749	1.2755	3.1
0	5	5	1.2347	1.2296	3.5
4	1	−5	1.2294	1.2272	3.2
2	5	−4	1.2184	1.2173	3.3
2	0	−8	1.2174		
1	5	5	1.2037	1.2023	6.4
2	3	−7	1.2003		
4	3	3	1.2000	1.2002	13.8
2	5	4	1.1997		
1	6	−3	1.1775	1.1775	9.6
3	0	7	1.1745	1.1739	12.8
2	6	0	1.1738		
1	6	3	1.1711	1.1712	8.8
2	4	6	1.1710		

Note. a = 6.0191(7) Å, b = 7.6494(7) Å, c = 10.465(1) Å, β = 92.39(1)°, $P2_1/n$, Z = 4.

The observed, calculated and difference neutron pattern of Ba_2VO_4 are plotted in Fig. 1. The fit is seen to be excellent. Data

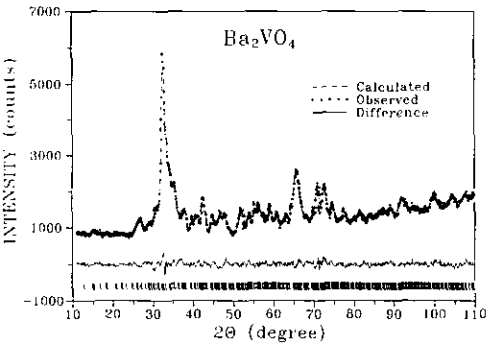

FIG. 1. Observed, calculated, and difference neutron powder pattern of β-Ba_2VO_4. Bragg peak positions are marked in the lower level as bars.

collection conditions and refinement details are summarized in Table II, and atomic parameters are listed in Table III. Because of the exceedingly small neutron scattering length of vanadium, its atomic position cannot be refined in the neutron profile refinement. The X-ray data refinement was used primarily to solve this problem. On the other hand, due to the existence of only a few intense reflections in the X-ray diffraction pattern and to the relatively poor profile data, oxygen positions could not be refined satisfactorily from the X-ray data. Thus the two methods are complementary. Positional parameters of oxygen atoms from the neutron profile refinement were used and held fixed in the X-ray data refinement. This was believed to be the major cause of their high temperature factors.

The crystal structure of Ba_2VO_4 is viewed along the b unique axis with VO_4^{4-} tetrahedra outlined as shown in Fig. 2. Selected bond distances and bond angles are listed in Table IV, together with those of the VO_4^{4-} polyhedra for β-Sr_2VO_4 for comparison. Unit cell parameters of interesting compounds are also compared in Table V. The structures of β-Ca_2SiO_4 (*5*) and β-Sr_2SiO_4 (*4*) models have been well described previously. The structural characteristics of

TABLE II

DATA COLLECTION CONDITIONS AND REFINEMENT DETAILS FOR Ba_2VO_4

	Neutron	X-ray
Cell parameters		
a(Å)	6.000(2)	6.025(1)
b(Å)	7.630(3)	7.661(2)
c(Å)	10.438(4)	10.486(3)
β(°)	92.36(2)	92.39(1)
V(Å^3)	477.4(5)	483.6(3)
2Θ range (°)	11–110	15–79
Step size (°)	0.10	0.030
Counting time (sec)	—	15
Nuclear R_N/Bragg R_B	0.0588	0.0477
Weighted profile R_{WP}	0.0403	0.0883
Profile R_P	0.0328	0.0696
Expected R_E	0.0228	0.0577
No. of profile points N	991	2134
No. of parameters refined	43	31
Independent reflections	423	316

$$R_N = R_B = \Sigma |I_{obs} - I_{cal}|/\Sigma I_{obs}$$

$$R_{WP} = \{[\Sigma w(Y_{obs} - Y_{cal}/c)^2]/\Sigma w Y_{obs}^2\}^{1/2}$$

$$R_P = \Sigma |Y_{obs} - Y_{cal}/c|/\Sigma Y_{obs}$$

$$R_E = [(N - P)/\Sigma w Y_{obs}^2]^{1/2}$$

Note. Space group $P2_1/n$, $Z = 4$.

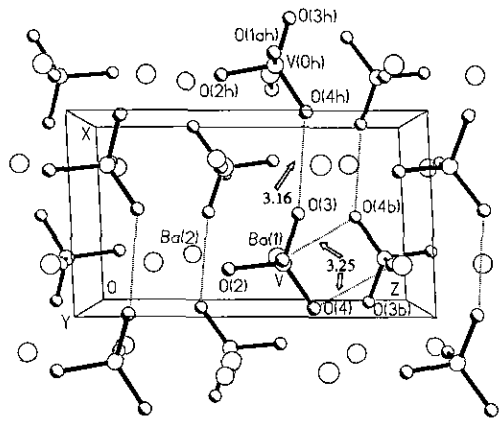

FIG. 2. Perspective view of the crystal structure of β-Ba_2VO_4 along the b-axis. Dotted lines represent the shortest and next shortest O–O contact distances.

Ba_2VO_4 can be summarized as consisting of isolated VO_4^{4-} and loosely bonded $Ba(1)O_{10}$ and $Ba(2)O_9$ polyhedra. The VO_4^{4-} tetrahedra are well separated with the shortest V–V distance of 4.74 Å. They are distributed in three dimensions such that no clear dimer, chain, or two-dimensional character is recognizable. The loose bonding nature of the Ba atoms in this structure can be seen from

TABLE III

ATOMIC PARAMETERS FOR Ba_2VO_4 FROM NEUTRON AND X-RAY (IN SQUARE BRACKETS) POWDER DIFFRACTION DATA

Atom	Site	x	y	z	B(Å^2)
Ba(1)	4(a)	0.259(2)	0.345(1)	0.576(1)	1.1(2)
		[0.261(2)	0.347(1)	0.5749(9)	3.7(4)]
Ba(2)	4(a)	0.263(2)	0.007(2)	0.3023(9)	0.9(2)
		[0.259(2)	−0.001(1)	0.3021(8)	4.4(4)]
V	4(a)	0.247	0.784	0.0206	1.8
		[0.247(4)	0.784(2)	0.0206(5)	1.8(7)]
O(1)	4(a)	0.273(2)	0.011(1)	0.5799(9)	2.3(2)
		[0.273	0.011	0.5799	9(2)]
O(2)	4(a)	0.212(2)	0.683(2)	0.4267(9)	1.4(2)
		[0.212	0.683	0.4267	9(2)]
O(3)	4(a)	0.495(2)	0.684(1)	0.636(1)	1.1(2)
		[0.495	0.684	0.636	9(2)]
O(4)	4(a)	0.018(2)	0.719(2)	0.671(1)	1.6(2)
		[0.018	0.719	0.671	9(2)]

TABLE IV

SELECTED BOND DISTANCES (Å) AND BOND ANGLES (°) IN β-Ba_2VO_4 AND β-Sr_2VO_4

		β-Sr_2VO_4	
V(1)–O(3)	1.88(2)	V(2)–O(1)	1.74(2)
V(1)–O(5)	1.75(2)	V(2)–O(2)	1.71(3)
V(1)–O(7)	1.76(2)	V(2)–O(4)	1.99(3)
V(1)–O(8)	1.65(3)	V(2)–O(6)	1.96(2)
		V(2)–O(3)	2.37(3)
Average	1.76(2)	tetrahedron	1.85(3)
		trigonal bipyramid	1.95(3)
O(3)–V(1)–O(5)	103(2)	O(1)–V(2)–O(2)	139(1)
O(3)–V(1)–O(7)	100(1)	O(1)–V(2)–O(3)	84(1)
O(3)–V(1)–O(8)	126(1)	O(1)–V(2)–O(4)	107(2)
O(5)–V(1)–O(7)	104(1)	O(1)–V(2)–O(6)	97(1)
O(5)–V(1)–O(8)	113(1)	O(2)–V(2)–O(3)	83(1)
O(7)–V(1)–O(8)	109(2)	O(2)–V(2)–O(4)	108(1)
		O(2)–V(2)–O(6)	98(1)
		O(3)–V(2)–O(4)	80(1)
		O(3)–V(2)–O(6)	177(2)
		O(4)–V(2)–O(6)	97(1)
Average	109(1)	tetrahedron	108(1)
		β-Ba_2VO_4[a]	
Ba(1)–O(1)	2.543(14)	Ba(2)–O(1)	2.896(13)
Ba(1)–O(2)	3.023(15)	Ba(2)–O(1)d	2.999(15)
Ba(1)–O(2)a	3.179(16)	Ba(2)–O(1)e	3.494(15)
Ba(1)–O(2)b	2.836(16)	Ba(2)–O(2)f	2.817(17)
Ba(1)–O(3)	3.006(15)	Ba(2)–O(2)g	2.750(15)
Ba(1)–O(3)a	2.716(15)	Ba(2)–O(3)a	2.827(16)
Ba(1)–O(3)c	3.640(16)	Ba(2)–O(3)h	2.742(15)
Ba(1)–O(4)	3.367(15)	Ba(2)–O(4)b	2.710(16)
Ba(1)–O(4)b	3.050(16)	Ba(2)–O(4)i	2.716(16)
Ba(1)–O(4)c	3.063(15)		
Average	3.042(16)		2.883(15)
		O(1)–V–O(2)	113.0(16)
		O(1)–V–O(3)	111.6(13)
V–O(1)	1.75(2)	O(1)–V–O(4)	112.1(14)
V–O(2)	1.84(3)	O(2)–V–O(3)	98.6(13)
V–O(3)	1.73(3)	O(2)–V–O(4)	106.3(13)
V–O(4)	1.73(3)	O(3)–V–O(4)	114.4(15)
Average	1.76(3)		109.3(14)

[a] Conventions for symmetry codes of β-Ba_2VO_4: a. (1 − X, 1 − Y, 1 − Z); b. (−X, 1 − Y, 1 − Z); c. (0.5 − X, −0.5 + Y, 1.5 − Z); d. (1 − X, −Y, 1 − Z); e. (−X, −Y, 1 − Z); f. (X, −1 + Y, Z); g. (0.5 − X, −0.5 + Y, 0.5 − Z); h. (−0.5 + X, 0.5 − Y, −0.5 + Z); i. (0.5 + X, 0.5 − Y, −0.5 + Z).

the Ba–O bond lengths. Ba(1)–O ranges from 2.54(1) to as long as 3.64(2) Å with an average value of 3.04 Å; Ba(2)–O from 2.71(2) to 3.49(2) Å with an average value of 2.81 Å. The shorter average Ba(2)–O bond length suggests a slightly tighter Ba(2)–O bonding. Similar trends have been observed for the alkaline earth metals in all of the monoclinic forms.

Although the structure of Ba_2VO_4 and that of β-Sr_2VO_4 (*1*) are both derived from the same β-K_2SO_4 type structure, there exists a significant difference between the VO_4^{4-} polyhedra of the two vanadium oxides. As can be seen in Table IV, the coordination polyhedron of V in β-Ba_2VO_4 is rather similar to that of V(1) in β-Sr_2VO_4. Both types of VO_4^{4-} polyhedra have one bond slightly longer than the other three, and the average V–O bond length of β-Ba_2VO_4, 1.76(3) Å, is the same as the V(1)–O of the β-Sr_2VO_4, 1.76(2) Å. Meanwhile, the O–V(1)–O bond angles vary from 100° to 126°, also similar to the VO_4^{4-} of β-Ba_2VO_4 which ranges from 99° to 114°. However, V(2) of the β-Sr_2VO_4 has a unique feature. In the first coordination sphere (bond length less than 2.0 Å), it is bonded to four oxygen atoms with V(2)–O distances ranging from 1.71(3) to 1.99(3) Å and an average of 1.85(3) Å, and bond angles ranging from 97° to 139°. Apparently $V(2)O_4^{4-}$ deviates from an ideal tetrahedron (~109.5°) far more severely than the other VO_4^{4-} polyhedra just discussed. Furthermore, V(2) seems to be loosely bonded to O(3) at a rather long distance of 2.37(3) Å as well. Similar long V–O bonds had been reported for some reduced VO_{2+x} oxides. For example, in V_4O_9 there is a long V–O bond for three of its four nonequivalent V atoms, which ranges from 2.23 to 2.50 Å (*16*).

Because O(3) is directly bonded to V(1), being the longest among the V(1)–O bonds, the V(1) and V(2) polyhedra can be viewed as linked by O(3) to form a $V_2O_8^{8-}$ dimer, and the V(2) coordination polyhedron can thus be described roughly as a trigonal bipyramid with average V(2)–O of 1.95 Å. Relevant bond distances and bond angles are also listed in Table IV. Such a molecular geometry is shown in Fig. 3. The packing of the dimers in the crystal structure as viewed perspectively along the shortest *b*-axis is shown in Fig. 4. It is worth emphasizing that the VO_4^{4-} polyhedra of β-Ba_2VO_4 are truly isolated because for the second coordination sphere even the

TABLE V

LATTICE PARAMETERS OF β-Ba_2VO_4 (GUINIER DATA) AND OTHER STRUCTURALLY RELATED OXIDES

Compound	a(Å)	b(Å)	c(Å)	β(°)	V(Å^3)	Comments	Reference
(β-)Ba_2TiO_4	6.1147(5)	7.6735(6)	10.5496(7)	93.182(6)	494.2		(*21*)
(α'-)Ba_2TiO_4	6.1069(5)	7.6514(6)	10.5502(7)	90	493.0		(*8*)
β-Ba_2VO_4	6.0191(7)	7.6494(7)	10.465(1)	92.39(1)	481.4	Slowly cooled	This work
	6.015(1)	7.643(1)	10.484(1)	92.31(2)	481.6	800°C quenched	This work
	6.014(1)	7.644(1)	10.495(1)	92.10(1)	482.1	1100°C quenched	This work
(α'-)Ba_2CrO_4	5.915(1)	7.627(1)	10.466(2)	90	472.2	Slowly cooled	(*20*)
(α'-)Ba_2SiO_4	5.805	7.498	10.198	90	443.9		(*3*)
(α'-)Ba_2GeO_4	5.982	7.576	10.417	90	472.1		(*3*)
β-Sr_2SiO_4	5.663(1)	7.084(2)	9.767(2)	92.67(2)	391.4		(*4*)
α'-Sr_2SiO_4	5.682	7.090	9.773	90	393.7		(*6*)
(α'-)Sr_2GeO_4	5.859	7.155	9.940	90	416.7		(*3*)
β-Ca_2SiO_4	5.502(1)	6.745(1)	9.297(1)	94.59(2)	343.9		(*5*)
α'-Ca_2SiO_4	5.59	6.85	9.49	90	363.0		(*6*)

Note. 1. Two more phases are known for Ca_2SiO_4 (6). 2. Space groups: the β-phase: $P2_1/n$ (No. 14), strongly deformed β-K_2SO_4 type structure; the α'-phase: *Pmnb* (No. 62), isostructural with β-K_2SO_4.

shortest V–O contact distance is as long as 3.76(1) Å.

The $V_2O_8^{8-}$ dimer description provides an alternate way of understanding the observed magnetic behavior of β-Sr_2VO_4 (*1*). The large V(1)–O(3)–V(2) bond angle of 147° should allow a reasonably good orbital overlapping. Thus this V(1)–O(3)–V(2) pathway is more likely responsible for the observed magnetic dimer behavior than the previously suggested V(1)–O(3)–O(1)–V(2) pathway.

Not surprisingly, all these VO_4^{4-} polyhedra are less regular than the SiO_4^{4-} polyhedra found in the β types of A_2SiO_4 (A = Ca, Sr). The SiO_4 polyhedra in the silicates are more similar to an ideal tetrahedron. For example, the Si–O distances range from

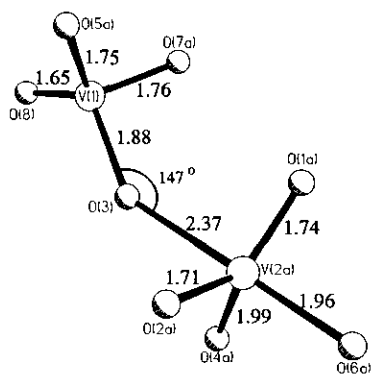

FIG. 3. Molecular geometry of a $V_2O_8^{8-}$ dimer in β-Sr_2VO_4.

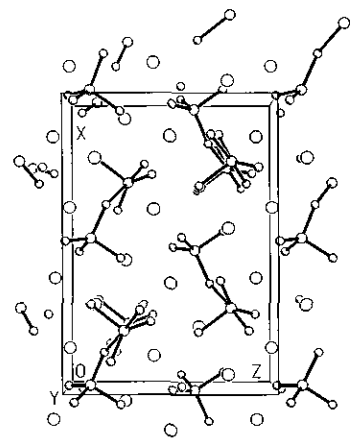

FIG. 4. Packing of $V_2O_8^{8-}$ dimers in β-Sr_2VO_4 as viewed along the b-axis.

1.61 to 1.65 Å (average 1.63) and the O–Si–O angles from 102.8 to 111.8° (average 109.5) for β-Ca_2SiO_4 (*5*).

It would be of interest to compare the structures of β-Ba_2VO_4 and monoclinic Ba_2TiO_4 (*7*). Unfortunately, the published structure for Ba_2TiO_4 is of low precision, rendering dubious any meaningful comparisons.

It is worth noting that the known compounds containing tetrahedral MO_4^{4-} for M = Ti, V, and Cr are mainly those of the large-sized Sr^{2+} and Ba^{2+}. For Ca^{2+} only octahedral and square pyramidal M–O coordination are known. For Sr tetrahedral M–O coordination has been found only for M = Cr (*17*) and V (*1*) in addition to other coordination types while Ba seems to favor only tetrahedral coordination for M under ambient pressure. This seems to suggest that increasing the size of the alkaline earth metal ion has the net effect of decreasing the internal packing pressure and thus favors the formation of 4-coordinated MO_4^{4-} polyhedra.

Magnetic Properties

Resistance measurements on sintered pellets with a typical size of 5 × 5 × 2 mm^3 by a two-probe method at room temperature indicated that Ba_2VO_4 is insulating with a bulk resistance >30 MΩ. There exists a broad maximum in the magnetic susceptibility curve of Ba_2VO_4 at ~11 K which indicates the presence of short range magnetic correlations. As would be expected from the above discussions of the crystal structures, the observed magnetic susceptibility data of Ba_2VO_4 cannot be fitted to a simple dimer model like β-Sr_2VO_4. An attempt to fit the data to a two dimensional (2D) Heisenberg model also failed. Both the dimer and 2D models predicted a significantly sharper maximum. The best fit was obtained using an $S = \frac{1}{2}$ one dimensional (1D) Heisenberg model. The equation used for the 1D fit can be written as

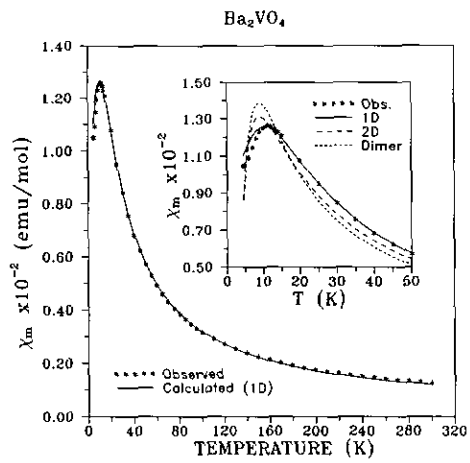

FIG. 5. Observed and calculated magnetic susceptibility curves for β-Ba_2VO_4.

$$\chi_m = \frac{N\bar{g}^2\mu_B^2}{kT} \cdot \frac{A + BX^{-1} + CX^{-2}}{1 + DX^{-1} + EX^{-2} + FX^{-3}} + \chi_{TIP},$$

where $X = kT/|J|$, $\bar{g}$ is the powder-averaged g-factor, and J is the exchange constant. The first term is from Hatfield (*18*) and evaluates the susceptibility for a 1D $S = \frac{1}{2}$ Heisenberg system. The last term corrects for temperature independent contributions. The following coefficients which were obtained from a fit of the 1D equation to a theoretical calculation for the $S = \frac{1}{2}$ Heisenberg system (*18*) were used in our calculation: $A = 0.25$, $B = 0.14995$, $C = 0.30094$, $D = 1.9862$, $E = 0.68854$, $F = 6.0626$. The fitting gave $\bar{g} = 1.91$, $J/k = -8.99$ K, and $\chi_{TIP} = 9.9 \times 10^{-5}$ $cm^3 \cdot mol^{-1}$ which are reasonable. The observed and calculated data are plotted in Fig. 5.

Since the VO_4^{4-} polyhedra in Ba_2VO_4 are isolated and their arrangement does not suggest any clear low dimensionality, it is not obvious why the structure displays quasi-one dimensional character as suggested by the magnetic data. The magnetic superexchange coupling must involve V–O–O–V or

more complicated V–O–Ba–O–V pathways. One possible mechanism that exhibits quasi-one dimensional character parallel to the *a* axis is outlined in Fig. 2. That is the V–O(3)–O(4h)–V(Oh) pathway which involves the shortest O–O distance and VO_4^{4-} groups from neighboring unit cells. Relevant distances (Å) are 1.73(3), 3.16(3), and 1.73(3) from left to right and bond angles (°) of 147(2) for V–O(3)–O(4h) and 140(2) for O(3)–O(4h)–V(Oh). Obviously the 1D model, though the best among those tried, cannot explain the magnetic behavior satisfactorily. As shown in the inserted graph in Fig. 5, the observed antiferromagnetic transition on the susceptibility curve is actually slightly sharper than that evaluated based on a simple 1D Heisenberg model. This is not surprising considering the fact that the arrangement of the tetrahedra is truly three dimensional. For example, the next shortest O–O distance, 3.25(3) Å, involves oxygen atoms from neighboring "chains."

Another notable difference between the magnetic behavior of β-Ba_2VO_4 and β-Sr_2VO_4 is the magnitude of the magnetic exchange constant. The exchange coupling constant of β-Ba_2VO_4 is only about $\frac{1}{6}$ of that for β-Sr_2VO_4 ($\bar{g} = 1.88$, $J/k = -52$ K). This result is again a reflection of the fact that the VO_4^{4-} polyhedra in β-Ba_2VO_4 are linked through a long O–O distance (3.16 Å), compared to that of the "dimer" in β-Sr_2VO_4.

The magnetization curve of β-Ba_2VO_4 at 5 K is presented in Fig. 6. No clear indication of a spin flop transition up to 4 T in Fig. 6 or a susceptibility anomaly below the χ_{max} temperature in Fig. 5 can be seen. Thus the magnetic data do not suggest long range magnetic order down to 5 K.

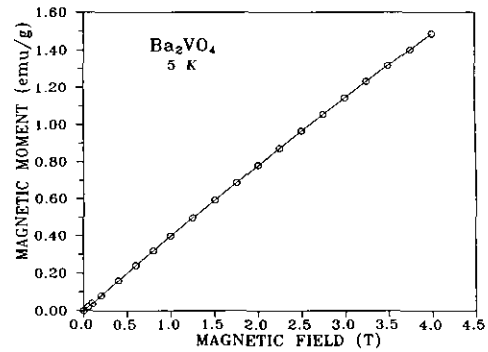

FIG. 6. Change in magnetic moment of β-Ba_2VO_4 as a function of applied magnetic field at 5 K.

Formation Mechanism of Ba_2VO_4

The synthesis of phase-pure Ba_2VO_4 turned out to be more difficult than the seemingly easy H_2 reduction indicated by the chemical equation

$$Ba_3V_2O_8(s) + BaCO_3(s) + H_2(g) \rightarrow 2Ba_2VO_4(s) + CO_2(s) + H_2O(g). \quad (1)$$

The reaction was strongly affected by the type of container used, and most importantly, the composition of the reactants as explained below. Other reaction routes such as the direct synthesis of Ba_2VO_4 by inductive heating of a 2BaO + VO_2 mixture in a sealed Mo tube failed because of the difficulty in handling the extremely air- and moisture-sensitive BaO. Hydrogen reductions of precursors of other combinations such as $Ba_3V_2O_8$ and $Ba(OH)_2$, $BaCO_3$ and $BaVO_3$ which was first made by reducing $Ba_2V_2O_7$ in hydrogen at 1200°C, and even $4BaCO_3$ and V_2O_3 obtained by hydrogen reduction of V_2O_5 at 650–750°C all resulted in the initial formation of $Ba_3V_2O_8$ and its subsequent reduction. Thus the route in Eq. (1) was chosen. $Ba_3V_2O_8$ alone cannot be reduced by hydrogen even at 1350°C. When a stoichiometric amount of $BaCO_3$ was used, $Ba_3V_2O_8$ was always observed in the final product even with repeated grinding and heating. The mass loss was always more than that expected according to Eq. (1). The possibility that the extra mass loss could be due to the formation of nonstoichiometric Ba_2-

VO_{4-x} cannot be ruled out completely. However, it is not likely because the composition Ba_2VO_{4-x} for $x > 0$ would require V^{3+} in four coordination which is highly unlikely. The loss of BaO probably occurred during the reaction through sublimation in the form of $Ba(OH)_2$ that could form from BaO and the moisture produced in the reaction. In fact, the deposition of unidentified white material was observed in the supporting alumina boat near the areas outside the molybdenum tube in which the reactants were confined. Thus the 20% excess $BaCO_3$ is necessary to force reaction (1) to completion. It is worth noting that higher concentrations of $BaCO_3$ (>1.5 mol) will lead to the contamination of the product by Ba_3VO_5. The existence of $BaCO_3$, which decomposes into BaO and CO_2 quickly at the reaction temperature in the presence of hydrogen, precluded the use of alumina boats as containers. The use of inert platinum crucibles, on the other hand, seemed to increase the loss of BaO. Finally, molybdenum was found to be an appropriate container material.

According to the studies on the silicates mentioned previously, amoung the various polymorphs, the monoclinic β-Sr_2SiO_4 and β-Ca_2SiO_4 are the lower-temperature phases and the orthorhombic a' forms are the higher-temperature phases (*6*). Monoclinic Ba_2TiO_4 can also be considered as the low-temperature normal phase; the high-temperature phase is again orthorhombic (*8*). It is interesting to note that Ba_2TiO_4 undergoes a Martensitic phase transition when cooled from high temperatures, and the high-temperature form can be stabilized at room temperature when prepared by the alkoxide precursor method (crystallized in a very fine-grained condition and the specimens were heat-treated overnight at 800°C) (*8*). Otherwise specimens of pure Ba_2TiO_4 exist as a mixture of both phases. Thus orthorhombic β-K_2SO_4 type Ba_2VO_4, if it exists, would be expected as the high-temperature form.

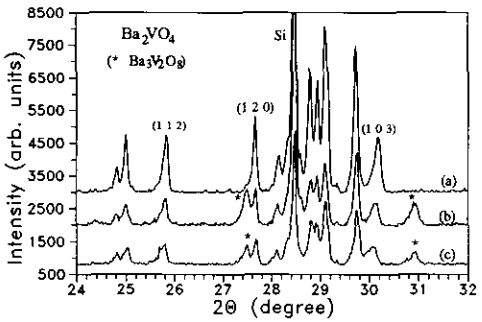

FIG. 7. Observed Guinier powder patterns of β-Ba_2VO_4. (Cu$K\alpha$1, λ = 1.5406 Å; Si internal standard.) (a) Slowly cooled hydrogen reduction product; (b) air-quenched at 800°C; (c) air-quenched at 1100°C.

Though an orthorhombic form of Ba_2VO_4 had been reported, the evidence provided is not convincing (*9*). In our experiment, the hydrogen reduction product was cooled slowly, and when a stoichiometric amount of $BaCO_3$ was used, the product always contained $Ba_3V_2O_8$. No such details were mentioned in the original paper but a similar method was used (hydrogen reduction of a $Ba_3V_2O_8$ and BaO mixture at 1100°C). In order to test the possible formation of orthorhombic Ba_2VO_4 during quenching, pelleted specimens of Ba_2VO_4 were sealed under a 10^{-4} Torr pressure in quartz, heated to 800°C and 1100°C for 1–2 hr, respectively, and then air quenched and the products examined by Guinier X-ray diffraction. In both cases the formation of a small amount of $Ba_3V_2O_8$ was observed. Diffraction patterns from scanned Guinier films are compared in Fig. 7. Several reflection peaks showed visible shifts, (1 0 3) being the most prominent, and (1 1 2) to a lesser extent. However, the symmetry of the Ba_2VO_4 phase remained monoclinic. Relevant lattice parameters are listed in Table V.

The above experimental results suggest that it is not likely that an orthorhombic form of Ba_2VO_4 could form during quenching. This led us to question the reliability of the previously assigned orthorhombic sym-

TABLE VI

OBSERVED AND CALCULATED INTERPLANAR *d*-SPACINGS AND INTENSITIES FOR "ORTHORHOMBIC" Ba_2VO_4: a = 6.056(4) Å, b = 7.702(5), c = 10.387(6), *Pmnb* (No. 62), Z = 4

h	k	l	d_{obs}	d_{cal}	I_{obs}	I_{cal}
1	0	1	5.24	5.232	7	8
1	1	1	—	4.328	—	16
0	1	2	4.30	4.306	6	6
0	2	1	3.60	3.611	15	8
(0	0	3)	3.46	3.509	19	81
1	2	0	3.255	3.2496	40	21
0	1	3	3.170	3.1579	40	22
1	2	1	3.120	3.1014	60	94
0	2	2	3.090	3.0934	100	40
2	0	0	3.024	3.028	65	84
1	0	3	2.976	3.0058	45	100
2	0	1	2.910	—	10	—
1	1	3	2.794	2.8001	7	<1

Note. The Miller indices are those reported (*10*); the lattice parameters were obtained by a least squares refinement using the reported *d*-spacings and by imposing the assigned Miller indices. Intensities were calculated based on the Ba_2CrO_4 model (*20*).

metry for Ba_2VO_4. First we attempted to index the *d*-spacings reported for the "orthorhombic" Ba_2VO_4 (*10*) by TREOR and no orthorhombic solution was obtained. Instead several monoclinic cells were suggested but all failed to index some of the given *d*-spacings. The reported data could be fitted to the orthorhombic cell parameters only when the assigned Miller indices were imposed. This gave a = 6.056(4) Å, b = 7.702(5) Å, and c = 10.387(6) Å, which are reasonably close to the reported values (*10*). However, the observed peaks matched poorly in both positions and intensities with those calculated using the program LAZY PULVERIX (*19*) and the refined orthorhombic Ba_2CrO_4 as the model (*20*). Some low angle reflections are compared in Table VI. The peaks which exhibit significant discrepancies are d_{obs} = 3.46 Å, 3.255, 3.120, 3.090 and 2.976; d_{obs} = 2.910 is not assignable to the Ba_2VO_4 phase at all. Based on the above results, we can conclude that the assignment of the orthorhombic symmetry for Ba_2VO_4 reported previously was in error. This was probably caused in part by the poor quality of the observed diffractometer data. It is also believed that their specimens were contaminated by $Ba_3V_2O_8$ because d_{obs} = 2.910 Å could be assigned to the second most intense reflection of $Ba_3V_2O_8$ (d = 2.8929 Å or 2θ = 30.89°; I = 75%), and the line at d_{obs} = 3.255 Å is very likely an overlap of the most intense peak of $Ba_3V_2O_8$ (d = 3.2475 or 2θ = 27.44; I = 100%) with the (1 2 0) reflection of β-Ba_2VO_4 (d = 3.2263 Å or 2θ = 27.63°; I = 38%). This can be seen clearly in Fig. 7.

These results, however, do not exclude the possible existence of an orthorhombic phase for Ba_2VO_4. It is worth noting that our quenching experiment results seem to suggest that the β angle decreases with increasing quenching temperature, and the unit cell dimensions increase (Table V). Given the fact that the orthorhombic phase for Ba_2TiO_4 and Ba_2CrO_4 (*20*) are known, the existence of orthorhombic Ba_2VO_4 as a high-temperature form is likely and the subject is worthy of further studies. Thermal analysis or *in situ* high-temperature X-ray diffraction would be likely to shed some light on this problem.

Acknowledgments

The financial support of the Natural Science and Engineering Research Council of Canada and the Ontario Centre for Materials Research is acknowledged gratefully. We thank Dr. J. Barbier for helpful discussions, Professor C. V. Stager for use of the magnetometer, and Mr. F. Gibbs for obtaining the TGA data.

References

1. W. GONG, J. E. GREEDAN, G. LIU, AND M. BJORGVINSSON, *J. Solid State Chem.* **95,** 213 (1991).
2. H.-P. GROßE AND E. TILLMANNS, *Cryst. Struct. Commun.* **3,** 599–605 (1974).
3. G. PIEPER, W. EYSEL, AND TH. HAHN, *J. Am. Ceram. Soc.* **55,** 619–622 (1972).
4. M. CATTI, G. GAZZONI, AND G. IVALDI. *Acta Crystallogr. Sect. C* **39,** 29–34 (1983).

5. K. H. JOST, B. ZIEMER, AND R. SEYDEL, *Acta Crystallogr. Sect. B* **33,** 1696–1700 (1977).
6. J. BARBIER AND B. G. HYDE, *Acta Crystallogr. Sect. B* **41,** 383–390 (1985).
7. J. A. BLAND, *Acta Crystallogr.* **14,** 875–881 (1961).
8. J. J. RITTER, R. S. ROTH, AND J. E. BLENDELL, *J. Am. Ceram. Soc.* **69,** 155 (1986); Powder Diffraction File card 38-1481. JCPDS: International Centre for Diffraction Data, 1601 Park Lane, Swarthmore, PA 19081.
9. A. FELTZ AND S. SCHMALFUß, *Z. Chem.* **15,** 289–291 (1975).
10. Powder Diffraction File card 32-91. JCPDS: International Centre for Diffraction Data, 1601 Park Lane, Swarthmore, PA 19081.
11. R. J. HILL AND C. J. HOWARD, Australian Atomic Energy Commission Report No. M112, Lucos Heights Research Laboratories, New South Wales, Australia (1986).
12. D. B. WILES AND R. A. YOUNG, *J. Appl. Crystallogr.* **14,** 149 (1981).
13. J. N. REIMERS, J. E. GREEDAN, AND M. SATO, *J. Solid State Chem.* **72,** 390 (1988).
14. V. F. SEARS, *in* "Methods of Experimental Physics" (K. Skold and D. L. Price, Eds.), Vol. 23a, p. 521, Academic Press, San Diego (1986).
15. P. E. WERNER, L. ERIKSSON, AND M. WESTDAHL, *J. Appl. Crystallogr.* **18,** 367 (1985).
16. K.-A. WILHELMI AND K. WALTERSSON, *Acta Chem. Scand.* **24,** 3409 (1970).
17. K.-A. WILHELMI. *Arkiv Kemi* **26,** 157 (1967).
18. W. E. HATFIELD, *J. Appl. Phys.* **52,** 1985 (1981).
19. K. YVON, W. JEITSCHKO, AND E. PARTHÉ, *J. Appl. Crystallogr.* **10,** 73 (1977).
20. G. LIU AND J. E. GREEDAN, submitted for publication.
21. Powder Diffraction File card 35-183. JCPDS: International Centre for Diffraction Data, 1601 Park Lane, Swarthmore, PA 19081.